JOURNAL OF GEOPHYSICAL RESEARCH: SPACE PHYSICS, VOL. 118, 4618–4627, doi:10.1002/jgra.50426, 2013

Investigations on vertical coupling of atmospheric regions using combined multiwavelength optical dayglow, magnetic, and radio measurements

Fazlul I. Laskar,[1] Duggirala Pallamraju,[1] T. Vijaya Lakshmi,[2] M. Anji Reddy,[2] B. M. Pathan,[3] and Supriya Chakrabarti[4]

Received 21 March 2013; revised 13 June 2013; accepted 27 June 2013; published 24 July 2013.

[1] Systematic investigations of optical dayglow emissions at OI 557.7, OI 630.0, and OI 777.4 nm have been carried out simultaneously over a large field of view (~140°). These emission intensities are obtained during January–March in the years 2011 and 2012 from Hyderabad (17.5°N, 78.5°E), India, using a high spectral resolution multiwavelength imaging echelle spectrograph. Spectral analyses of planetary wave type periodicities in all the dayglow emission intensities are performed, and their association with lower atmospheric and direct solar forcings is presented. This analysis revealed that periods near the atmospheric free normal modes of 5, 10, 16, and 25 days (which are produced mainly in the troposphere) are found to register their presence in the upper atmospheric emission intensities. In an earlier study during high solar activity period (2001), sunspot numbers (SSNs) and the daily averaged OI 630.0 nm dayglow intensities were seen to be covarying. In contrast, the variability in the dayglow emission intensities during relatively low solar activity epoch (2011) shows no or weaker correlation with that of the SSN but a greater similarity with that of the equatorial electrojet strength. Periodicities of both lower atmospheric normal modes and those related to sunspots are found during moderate solar activity (2012). Based on this analysis, it appears that the upper atmospheric dayglow emissions respond mainly to lower atmospheric forcing during low solar activity, solar forcing in high solar activity, and both during moderate solar activity level.

Citation: Laskar, F. I., D. Pallamraju, T. V. Lakshmi, M. A. Reddy, B. M. Pathan, and S. Chakrabarti (2013), Investigations on vertical coupling of atmospheric regions using combined multiwavelength optical dayglow, magnetic, and radio measurements, *J. Geophys. Res. Space Physics*, *118*, 4618–4627, doi:10.1002/jgra.50426.

1. Introduction

[2] The upper atmosphere of the Earth receives energy inputs from the incoming solar radiation and by the breaking of waves that propagate upward from the lower atmosphere. The solar influence is in terms of the electromagnetic (extreme ultraviolet, X-ray) and corpuscular radiation (particle precipitation). For a long time, it was considered that various layers behave differently due to different physical processes that occur in those altitudes. However, with the advent of various advanced ground- and satellite-based measurements, which provide information on the temporal variation and altitude structure of a given parameter for a given location, it is found that various layers are, to a significant extent, dynamically coupled [e.g., *Immel et al*., 2006; *Pallamraju et al*., 2012]. The dynamical coupling between lower and upper atmospheres can happen by the propagation of waves of various periods and scale sizes. The wave influence is mainly through the dissipation of gravity waves (GWs) [e.g., *Hines*, 1960; *Hocke and Schlegel*, 1996; *Fritts and Alexander*, 2003], tides [e.g., *Forbes*, 1982; *Pedatella and Forbes*, 2010], and planetary waves (PWs) [e.g., *Salby*, 1984; *Forbes et al*., 1995; *Pancheva et al*., 2008]. The wave dynamics in the upper atmosphere can be due to the superposition of waves due to all the sources mentioned above.

[3] PWs are global-scale oscillations in the neutral atmosphere with periods between 2 and 30 days [*Salby*, 1984] and wavelengths on the order of the radius of the Earth. The most commonly observed PWs which, in general, are produced in the troposphere are of periods that are around 2, 5, 10, 16, and 25 days. These PWs are identified as manifestations of the normal modes of the atmosphere [*Salby*, 1984]. From a numerical study, *Salby* [1984] had shown that depending on the background atmospheric conditions, such as nonisothermality, magnitude, and direction of winds, these normal modes can undergo spectral broadening, dissipation, and Doppler shifts.

[1]Space and Atmospheric Sciences Division, Physical Research Laboratory, Ahmedabad, India.
[2]Center for Environment, Jawaharlal Nehru Technological University, Hyderabad, India.
[3]Indian Institute of Geomagnetism, Navi Mumbai, India.
[4]Department of Physics and Applied Physics, University of Massachusetts Lowell, Lowell, Massachusetts, USA.

Corresponding author: D. Pallamraju, Space and Atmospheric Sciences Division, Physical Research Laboratory, Navrangpura, Ahmedabad, Gujarat 380009, India. (raju@prl.res.in)

2169-9380/13/10.1002/jgra.50426

[4] The 5 day wave is generally referred to as a westward propagating rotational Rossby mode wave of wave number 1 and having a period of 4–6.5 days [*Salby*, 1984; *Meyer and Forbes*, 1997; *Niranjan Kumar et al*., 2012; *Sassi et al*., 2012]. The 10 day (theoretically, 8.3–10.6 days [*Salby*, 1984]) wave is also a westward propagating Rossby normal mode of wavenumber 1. The 16 day wave is the second symmetric Rossby normal-mode resonant oscillation of the atmosphere. Depending on the background atmospheric conditions, the 16 day wave can have periods between 11.2 and 20 days with the 16 day as median value [*Salby*, 1984]. The 25 day wave is also a normal mode and may be distorted by the background flow due to its slow movement.

[5] The behavior of these PWs or Rossby normal modes shows dramatic features, such as amplification and propagation to the upper atmosphere etc., during the Stratospheric Sudden Warming (SSW) events. SSW is a very large-scale global phenomenon which occurs particularly in the Northern Hemispheric wintertime. It is believed to be produced due to the interaction of wintertime-enhanced PWs with the mean zonal flow. This interaction results in the amplification of PWs and consequent heating of the stratosphere in the Northern Hemispheric high latitudes [*Matsuno*, 1971; *Chau et al*., 2012]. Though the SSW is a polar latitude event, it is found that it influences the dynamics of the low-latitude atmosphere-ionosphere system significantly through atmospheric coupling [e.g., *Fejer*, 2011; *Chau et al*., 2012; *Guharay and Sekar*, 2012], in particular the 16 day mode PW has been found to be highly associated with SSW activity [*Pancheva et al*., 2008].

[6] The dynamical coupling between the lower and the upper atmosphere in terms of PWs has been a subject of intense research (see review by *Fejer* [2011]). From theoretical and modeling studies, it is demonstrated that the PWs do not propagate directly above about 100–110 km [*Pogoreltsev et al*., 2007]. However, their influence is communicated through their interaction with other dynamical features and is reported in various parameters in the mesosphere-lower thermosphere (MLT) and Ionosphere (MLTI) regions, such as mesospheric wind [e.g., *Gurubaran et al*., 2001], mesospheric temperature [e.g., *Sassi et al*., 2012], total electron content (TEC) [e.g., *Goncharenko et al*., 2010; *Sripathi and Bhattacharyya*, 2012], mesospheric airglow [*Takahashi et al*., 2002], equatorial electrojet strength (EEJ) [e.g., *Parish et al*., 1994; *Abdu et al*., 2006; *Vineeth et al*., 2007], and *F* region ionospheric parameters [e.g., *Fejer*, 2011; *Chau et al*., 2012]. It is suggested that the PW influence is transmitted to the MLT region by three possible mechanisms: (i) through interaction with propagating gravity waves, (ii) through interaction with tidal waves, and (iii) through the electrodynamical coupling in the *E* region (80–120 km) of equatorial latitudes. This third mechanism, in turn, contributes to the modification of several equatorial and low-latitude phenomena such as the equatorial ionization anomaly (EIA) and the equatorial temperature and wind anomaly. The most commonly observed MLTI region PWs have periods near 2, 4, 5, 8, 10, 12, 14, 16, and 24 days [e.g., *Goncharenko et al*., 2013].

[7] While long-period tidal and PW-type variations of periods 2–30 days can be studied using satellite-based measurements of atmospheric parameters, simultaneous ground-based measurements of emissions originating at multiple altitudes have the advantage that they provide information at a high temporal cadence on the wave dynamics that are present at those altitudes at the same time. The importance of the ground-based investigations of the daytime upper atmospheric dynamics has, in the recent past, been gaining momentum, especially due to several results that showed an influence of daytime upper atmospheric phenomena on the nighttime plasma processes [e.g., *Raghavarao et al*., 1988; *Sridharan et al*., 1994; *Pallam Raju et al*., 1996; *Valladares et al*., 2001; *Pallamraju et al*., 2004, 2010; *Pallamraju and Chakrabarti*, 2005; *Prakash et al*., 2009].

[8] The objective of this study is to characterize the upper atmospheric response to various forcings from above (solar input) as well as below (waves in general). In this regard, an effort has been made to investigate the dynamical coupling between lower and upper atmospheres in terms of PW signatures during different levels of solar activity. The wave dynamical behaviors of atmospheres at various altitudes are investigated for interrelationships and compared with the influence of solar variability to assess the relative response of the upper atmospheric behavior to the solar versus the lower atmospheric influences.

2. Data

[9] To study the vertical coupling of atmospheric regions, measurements representing different altitudes of atmosphere are considered in this paper. The dayglow emission intensities at OI 557.7, OI 630.0, and OI 777.4 nm represent the behavior of the altitudes from where they emanate, which are approximately 130 km, 230 km, and peak height of the *F* region, respectively [*Kulkarni*, 1976; *Solomon and Abreu*, 1989; *Zhang and Shepherd*, 2004, 2005; *Pallamraju et al*., 2013]. TEC is known to represent the variability of the peak height of the ionosphere and of above. The variability of dayglow emission intensities and the TEC represent the behavior of neutrals and plasma in the upper atmosphere. The variability of the EEJ strength (which originates at around 102 km altitude) and National Centers for Environmental Prediction (NCEP)/National Center for Atmospheric Research (NCAR) zonal winds at 10 hPa level (typically at around 30 km) represents the behavior of the MLT and lower atmospheric regions, respectively. The details of these data are explained in the following subsections.

2.1. Dayglow

[10] The dayglow emission intensities are derived from the spectral images of multiwavelength imaging spectrograph using echelle grating (MISE) [*Pallamraju et al*., 2013]. MISE is a long-slit echelle spectrograph designed to achieve spectral resolutions of 0.012, 0.015, and 0.018 nm at 557.7, 630.0, and 777.4 nm, respectively. MISE obtains a spectral image of the sky over a large field of view (FOV) (of about 140°) onto a 1 k × 1 k pixel charge-coupled device (CCD) detector. Owing to the imaging property of this instrument, different sections of the image on the CCD along the orientation of the slit map to different spatial regions in the sky. For example, for an emission altitude of 230 km for OI 630.0 nm dayglow emission, the spatial region covered is from 4°N to 13°N magnetic latitude (MLAT), when operated from Hyderabad (8.6°N MLAT) in India. Figure 1 presents a schematic of the viewing geometry and approximate peak heights

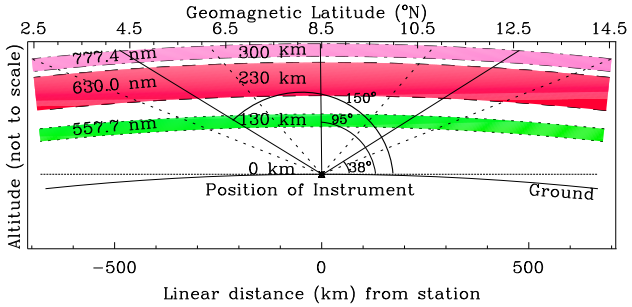

Figure 1. Schematic of the MISE sky viewing geometry. Different dayglow layers and their average altitudes from which the OI 557.7, OI 630.0, and OI 777.4 nm emissions emanate are shown. The spatial average of the three viewing directions correspond to elevation angles of approximately 38°, 95°, and 150° with respect to the northern horizon. It can be seen that for this FOV (~140°), the latitude extent covered for OI 557.7, OI 630.0, and OI 777.4 nm are about 5°, 9°, and 11°, respectively, at their respective heights. Note that the *y* axis is not to the scale and shows the approximate heights of the layer at 130, 230, and 300 km.

of all the three emissions. The data from different rows on the CCD chip of each image have been organized into three different sections (view directions) and averaged so that the spectra thus obtained correspond to the emissions in the sky centered at around 5.5°N, 8.5°N, and 11.5°N MLAT for the OI 630.0 nm emissions. These sky spectra are compared with a normalized solar spectrum [*Delbouille et al*., 1973] in wavelength and scaled at the continuum level so that the difference between them yields the emission brightness. This emission brightness contains contributions of both dayglow and scattering (Ring effect [*Grainger and Ring*, 1962]). For the removal of ring effect contribution from the emission region, a neighboring Fraunhofer spectral feature is considered where there are no emissions or telluric absorptions. A greater description of this technique and the method of data analysis have been reported earlier [*Pallamraju et al*., 2000, 2002, 2013]. For this study, the data corresponding to 38° elevation angle (with respect to the north) are used as in this viewing direction data gap due to the direct solar light and solar glare affecting the measurements is minimal. The dayglow measured with this instrument for January–March of 2011 and 2012 is used here. As the investigations in this study pertain to the effect of large (planetary wave) scale size waves on the upper atmosphere, the results are expected to be independent of the view orientation of dayglow emission intensity chosen.

2.2. TEC

[11] The TEC data are derived using the open-source global positioning system (GPS) toolkit (GPSTk) [*Harris and Mach*, 2007]. The GPSTk is used to process receiver-independent exchange (RINEX) format data provided by the International GNSS Service (IGS) [*Dow et al*., 2009]. The 30 s time resolution RINEX data are archived at Scripps Orbit and Permanent Array Center (http://sopac.ucsd.edu/cgi-bin/dbDataBySite.cgi) of the University of California, San Diego. The monthly satellite differential code bias is obtained from the University of Bern (ftp://ftp.unibe.ch/aiub/CODE/). As suggested by *Rama Rao et al*. [2006], the data from GPS satellites with elevation angles greater than 50° are considered for this analysis, which removes the dependence of TEC on ionospheric pierce point height [*Rama Rao et al*., 2006] and latitude, in addition to multipath effect.

[12] During our observation period, GPS-TEC data from stations in the vicinity of Northern Hemisphere's crest location of the EIA were either irregular or not available. So, as the winter anomaly subsided in this low solar epoch [e.g., *Nanan et al*., 2012], TEC data from a magnetically conjugate location in the Southern Hemisphere, (Diego Garcia: geographical latitude 7.27°S, longitude 72.4°E; 15.3°S MLAT) are used. Moreover, comparisons of the standard score of the hourly averaged daily afternoon TEC from a GPS receiver near the Northern Hemisphere EIA crest region showed similar temporal variations (not presented here) with that of the Diego Garcia. In fact, for the year 2011, the standard score of the common data from the two stations exactly overlay on each other. For the year 2012, there were minor differences at smaller timescales (periods of 2–3 days).

2.3. EEJ Strength

[13] Horizontal component of geomagnetic field (H) data at 1 min resolution is collected with magnetometers located at the equatorial station, Tirunelveli (TIR) (geographical latitude 8.7°N, longitude 77.7°E; 0.1°N MLAT) and off-equatorial station, Alibag (ABG) (geographical latitude 18.6°N, longitude 72.9°E; 10.3°N MLAT). To estimate the strength of the EEJ-induced magnetic field on the ground in the Indian longitudes, variations of H relative to its nighttime values at Alibag (ΔH_{ABG}) are subtracted from the corresponding values at Tirunelveli (ΔH_{TIR}), $\Delta H_{TIR} - \Delta H_{ABG}$.

2.4. NCEP/NCAR Reanalysis Wind

[14] The National Centers for Environmental Prediction (NCEP) and National Center for Atmospheric Research (NCAR) have cooperated in a project (denoted "reanalysis"), which involves the recovery of land surface, ship, rawinsonde, pibal, aircraft, satellite, and other data [*Kalnay et al*., 1996]. Daily averaged and 4-times-a-day data are available at 2.5°× 2.5° grid for the whole globe and for 17 pressure levels from the Earth's surface up to 10 hPa. For the current study, the zonal wind at 10 hPa (which approximately corresponds to an altitude of 30 km) is used to assess the characteristics of the PWs in the lower atmosphere.

3. Results and Discussion

[15] Figure 2 shows all the clear sky days' dayglow data of January–March for the years 2011 (left panel) and 2012 (right panel). Figures 2a and 2d, 2b and 2e, and 2c and 2f show daily dayglow emission intensity variations in Rayleighs at OI 557.7, OI 630.0, and OI 777.4 nm, respectively. The data gap during noontime is due to strong solar glare which enters directly into the slit of the spectrograph and saturates the CCD. For the dayglow emission intensities, the durations covered in this study are from day of the year (DOY) 7 to 90 for 2011 and from DOY 12 to 85 for 2012 covering 52 and 35 days in those years. The production mechanisms for the OI 630.0 nm emissions are photoelectron impact on O, photodissociation of O_2, and dissociative recombination of O_2^+ [*Solomon and Abreu*, 1989]. Typical red line emission (OI 630.0 nm) has a layer width of ~100 km

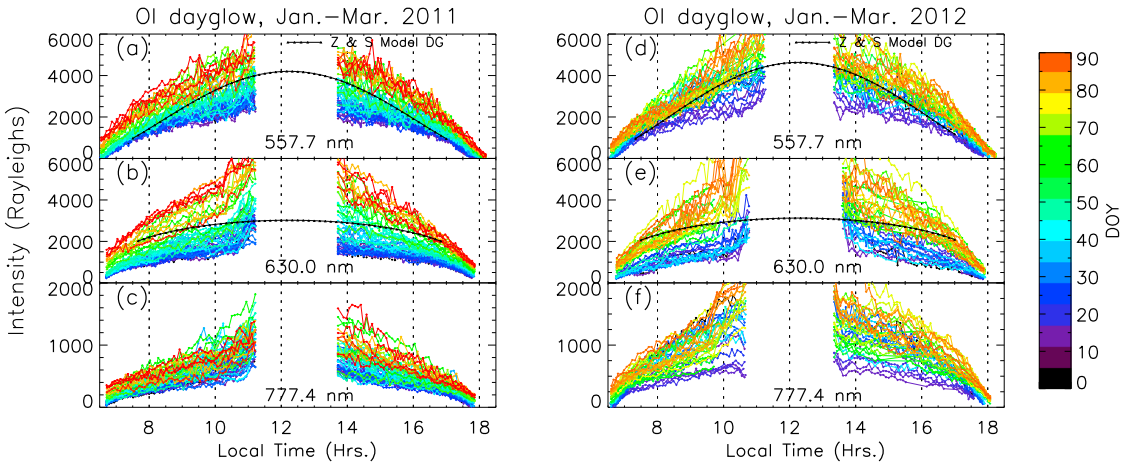

Figure 2. The daily dayglow emission intensities at the three wavelengths: (a and d) OI 557.7 nm, (b and e) OI 630.0 nm, and (c and f) OI 777.4 nm, for all the clear sky days during January–March of (left panels) 2011 and (right panels) 2012 are shown for the 38° elevation angle direction. Days covered in this study are from DOY 7 to 90 for 2011 and from DOY 12 to 85 for 2012. The smooth curves in the top and middle panels are the dayglow emissions as estimated using the Zhang and Shepherd empirical model [*Zhang and Shepherd*, 2004, 2005] for DOY = 40. It can be noted that the dayglow emission intensities are higher in 2012 due to higher solar activity as compared to 2011.

centered at around 230 km. The green line emission (OI 557.7 nm) has a sharp peak at around 100 km which is due to the three-body collision mechanism [*Barth and Hildebrandt*, 1961] and a broad peak near 150 km which is mainly due to collisional deactivation of $N_2(A)$ by O, the $N_2(A)$ being produced by photoelectron impact: $N_2(A) + O \rightarrow N_2 + O(^1S)$ [*Zhang and Shepherd*, 2005]. The OI 777.4 nm emission is due to radiative recombination of O^+, which, being a very slow process, yields emission intensities that are smaller in magnitude than those of the green and redline emissions. As the production mechanisms are dependent on the solar ionizing radiation available at a given location, the solar zenith angle (SZA)-dependent variation is an inherent feature as can be seen in Figure 2. In addition to the SZA-dependent variation, the dayglow intensity variations are also expected to contain the neutral dynamical features of both shorter-scale (gravity wave) and longer-scale (planetary wave) periodicities. There are periodicities in the gravity wave regime (few minutes to few hours) in all these emissions, which will be discussed in a future article as the focus of this study is to investigate the large-timescale (order of days) behavior. The solid black lines in Figures 2a and 2d, and 2b and 2e are the empirical model predictions for OI 557.7 and OI 630.0 nm, respectively, as presented by *Zhang and Shepherd* [2004, 2005]. These models are based on measurements made by WIND Imaging Interferometer onboard the Upper Atmosphere Research Satellite (UARS). The inputs to these empirical models are the SZA and solar F10.7 cm flux on that day. It may be noted that these models are applicable for SZA < 80°.

[16] The daily variation of dayglow intensities averaged during various local time hours revealed that the PW-type periods near 5, 10, and 16 days are found to be present at all local times from morning to evening (not shown here). However, only the averaged afternoon (1430 to 1730 local time (LT)) dayglow intensity data are used here, as the data during this period have fewer gaps and are present for greater number of days. Figure 3a shows the dayglow emission intensities at the three wavelengths, Figure 3b shows the daytime peak EEJ strength values, and Figure 3c depicts the TEC and daily SSN values. The left panels are for the year 2011 and the right panels are for that of 2012. These two data durations in 2011 and 2012 have almost the same SZA variation but have different solar activity levels. SZA at 1600 LT (average of 1430 to 1730 LT) of each day is plotted in the top panels as the dashed curve. Other than those due to the SZA variation, the gross increase in the magnitudes of dayglow emission intensities and the TEC values as seen in 2012 are mainly in response to the increased solar activity. The TEC values show similar behavior with that of the SSN in 2011 to a larger extent as compared to 2012. Lesser similarity of TEC with SSN in 2012 may be due to the mixed influences of solar and lower atmospheric wave activity, which will be described in the next section. At a first look, the 2011 dayglow variations show relatively greater resemblance with that of the EEJ strengths as opposed to that of the SSN. This is in contrast with a previous study using OI 630.0 nm dayglow, EEJ, and SSN variations obtained during the high solar activity period of 2001 as shown by *Pallamraju et al.* [2010]. That result is reproduced here as Figure 4, wherein OI 630.0 nm dayglow intensities were obtained from Carmen Alto (23.1°S, 70.6°W; 10.6°S MLAT) in Chile. Carmen Alto is located in similar magnetic latitude as the present observing station, Hyderabad, but in the Southern Hemisphere. *Pallamraju et al.* [2010] found that the OI 630.0 nm dayglow emission intensity variations in 2001 followed very closely with those of the SSN and not the EEJ. EEJ in the American longitudes had been obtained by subtracting the ΔH values obtained over a low-geomagnetic latitude station, Piura (Piu), from those of the equatorial station Jicamarca (Jic) ($\Delta H_{Jic} - \Delta H_{Piu}$). The authors showed that the solar periodicities of 9–12, 12–15, and 24 days were present in the OI 630.0 nm dayglow data, which were not seen in the EEJ strength. As the 630.0 nm

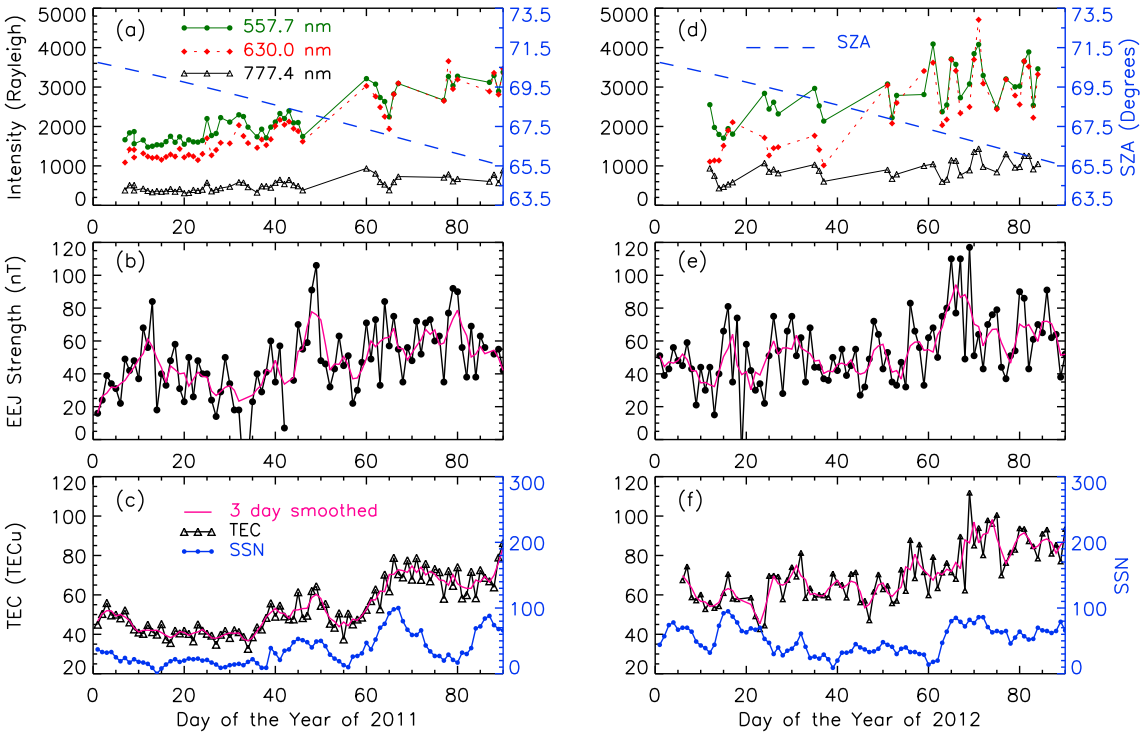

Figure 3. (a and d) Daily variations of dayglow intensities averaged during 1430–1730 LT for (left panels) 2011 and (right panels) 2012. The dashed lines in Figures 3a and 3d are the solar zenith angles at 1600 LT. (b and e) The daytime peak EEJ variations. (c and f) TEC values in TEC unit (TECu, 1 TECu = 10^{16} electrons/m^2) averaged during 1430–1730 LT and SSN. The 3 day moving average curves are overplotted in red for EEJ strength and TEC data. While calculating this running mean of EEJ strength, the DOY 33 and 34 (SSW days) of 2011 and DOY 24 (magnetic storm of DST index of −90 nT) of 2012 are excluded.

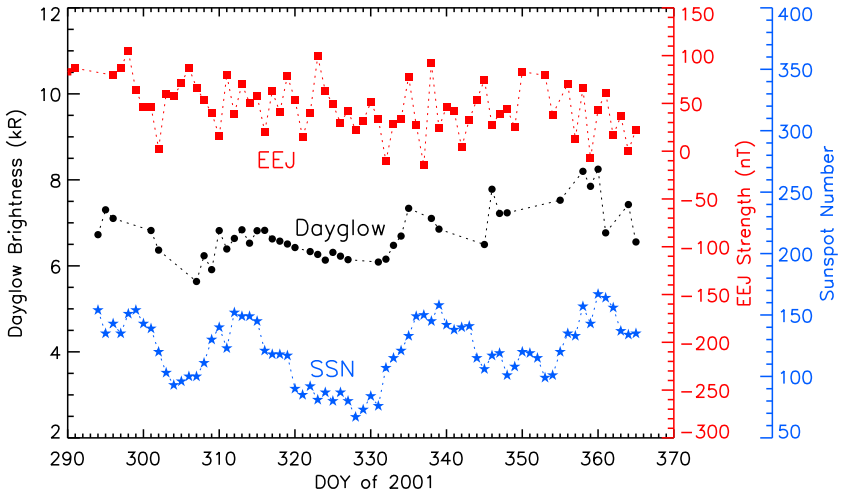

Figure 4. Variation of the daily averaged intensity of the OI 630.0 nm dayglow emissions as obtained from Carmen Alto, Chile, which has similar magnetic latitude (10.5°S) as that of the Hyderabad (8.5°N). The daily sunspot numbers and daily averaged equatorial electrojet strengths obtained by $\Delta H_{\mathrm{Jic}} - \Delta H_{\mathrm{Piu}}$ are also shown. The averaged dayglow emission brightness varies almost in phase with that of the daily sunspot number and not the EEJ, indicating that the long-timescale variability in the emissions is controlled by the variation in the solar flux (reproduced from our earlier work [*Pallamraju et al.*, 2010]).

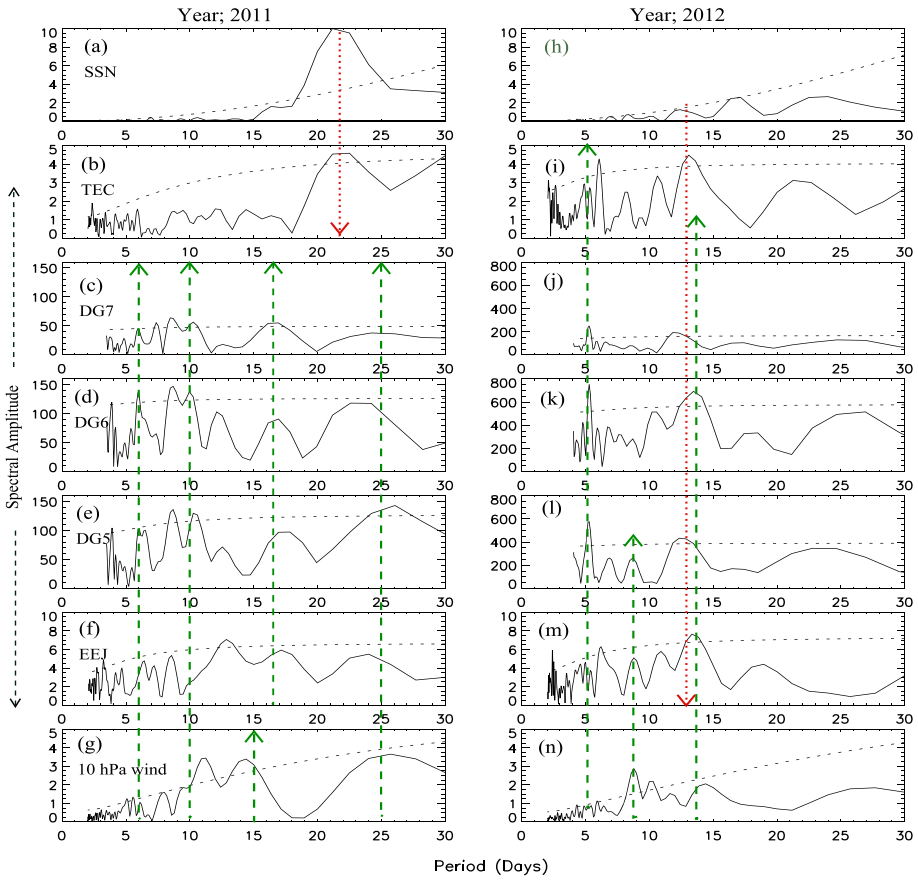

Figure 5. Normalized Lomb-Scargle periodograms are depicted for the parameters shown in Figure 3. (a–g) Periodograms of SSN, TEC, OI 777.4 nm dayglow, OI 630.0 nm dayglow, OI 557.7 nm dayglow, EEJ strength, and 10 hPa zonal wind, respectively, for the year 2011. (h–n) Periodograms of the same parameters for 2012. The tags DG5, DG6, and DG7 stand for the dayglow intensities of the OI 557.7, OI 630.0, and OI 777.4 nm emission lines, respectively. The dashed curves are the 90% FAL. Here the vertical arrows are traced to aid the eye and to show the direction of influence, upward arrow (dashed) indicate waves of lower atmospheric origin into the upper atmosphere, and the downward arrows (dotted) for the solar forcing on the upper atmosphere. It can be noted that the 5–6, 8–11, quasi-16, and 25 day periods are present in all the atmospheric parameters and the 22 day period is present in SSN and TEC in 2011. In the case of 2012, there are mixed responses seen. Periodicities of 5–6 and quasi-16 days are present in all the atmospheric parameters. However, the quasi-16 day period seen in the upper atmosphere could be an influence from lower atmospheric origin below or from above due to direct solar forcing.

dayglow production mechanisms depend on photoelectron and extreme ultraviolet (EUV) fluxes, the covariability in dayglow and SSN was found to be consistent. However, in the present analysis of the data of 2011, the situation seems different, most likely due to the lower solar activity during the year 2011 as compared to 2001. As the variations in the dayglow emissions at different levels of solar activity show similarity with lower atmospheric and solar-related variations to varying degrees, possible influences from the lower atmosphere and direct solar forcing have been investigated.

3.1. Forcing From Lower Atmosphere and Solar Flux

[17] It is known that the temporal variation of various solar parameters such as SSN, F10.7 cm flux, and EUV flux varies in a similar fashion. However, in order to compare with the earlier published data, we have used variations in SSN in this study. To quantify the variability seen in our data, Lomb-Scargle periodogram analysis has been carried out [*Lomb*, 1976; *Horne and Baliunas*, 1986]. Figure 5 shows the periodograms (solid lines) for all the data shown in Figure 3 along with their respective 90% false alarm level (FAL; dashed lines). Also, to investigate the possible wave activity in the lower atmosphere, the zonal winds at 10 hPa pressure level are also considered for analysis. Figures 5a–5g show the periodograms of SSN, TEC, OI 777.4 nm dayglow intensity, OI 630.0 nm dayglow intensity, and OI 557.7 nm dayglow intensity, EEJ strength, and zonal wind at 10 hPa level, respectively, for 2011. Similarly, Figures 5h–5n show periodograms of these parameters for 2012. One can note that there are striking similarities in the periodicities nearly at 5–6, 8–11, and 15–17 days between EEJ, OI 557.7 nm emission intensity, OI 630.0 nm emission intensity, and OI 777.4 nm emission intensity, and in TEC, to a minor extent (although the amplitude in some cases is slightly below the 90% FAL). These 5–6, 8–11, and 15–17 day periodicities are most likely due to 5, 10, and

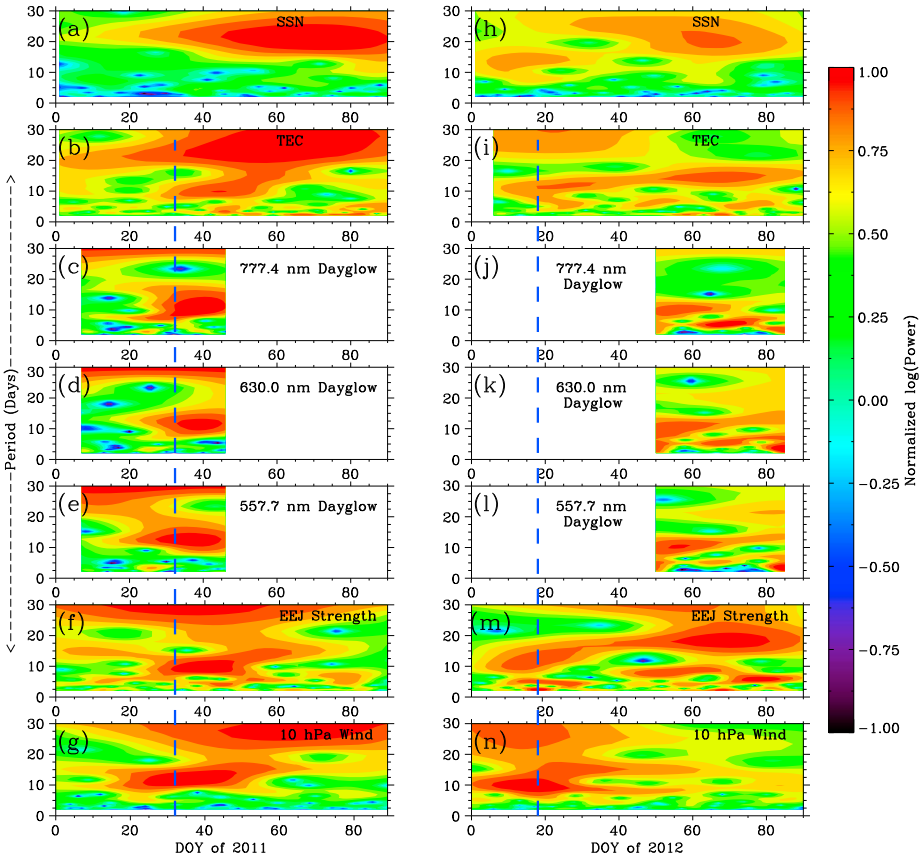

Figure 6. Normalized wavelet spectra showing the temporal occurrence of the periods seen in Figure 5. One can note that the 5–6, 8–11, and quasi-16 day periodicities occur in the same time duration in all the lower and upper atmospheric parameters, especially, (a–g) in 2011 indicating lower atmospheric influence on the upper atmosphere. (h–n) In 2012 data, 5–6 and 8–10 day periodicities during DOY 51–85 in all the atmospheric parameters and to some extent in SSN occur simultaneously. The concomitant occurrence of the quasi-16 day period between the DOY 5 and 35 in 10 hPa wind, EEJ, TEC, and SSN implies a possible mixed influence from both solar and lower atmosphere on the upper atmosphere in 2012. The two vertical dashed lines mark the onset of the minor SSW. In both years, the 8–10 day and quasi-16 day waves are seen to arise well before the onset of the minor SSW event.

16 day free normal modes, respectively. The zonal wind around our observation location (averaged over 10°N–20°N latitude, 75°E–85°E longitude, and at 10 hPa pressure level which corresponds to about 30 km altitude, obtained from NCAR/NCEP reanalysis) is treated as an indicator of the presence of the stratospheric planetary wave activity [*Sassi et al.*, 2012]. The periodicities of 5–6, 8–11, and quasi-16 days (11.2–20 days) that are seen in dayglow emission intensities and in the EEJ strength are also seen to be present in the low-latitude zonal wind at 10 hPa level for the year 2011 (upward dashed arrows are drawn to aid the eye to show the possible forcing from below). It is striking to note this similarity, in spite of the fact that these are independent measurements and they result from different processes. Although the power level of the 25 day period is slightly lower than the 90% FAL, it is striking to note that its presence is seen in all the lower and upper atmospheric data sets. It may seem that the 24–25 day periodicity in the all the atmospheric parameters (except the TEC) is due to Doppler shifted period of the solar 22 day period. However, it is believed that this is unlikely the case, as (a) the TEC which is an atmospheric parameter responds to the solar 22 day variation, while the other parameters do not, and (b) it is known that the 25 day is a normal mode oscillation of the lower atmosphere [*Sassi et al.*, 2012]. In 2011, when the solar activity level was relatively lower (average SSN = 35) as compared with that of 2001 (average SSN = 123), it seems that the forcings due to lower atmospheric components in the upper atmosphere are dominant. Further, as all the atmospheric parameters reported here are of different types with their own individual sources of productions or variations and they can have different damping and dissipation rates at their respective altitudes [*Salby*, 1984], one may not expect commensurate amplifications in the amplitudes of the periods in these parameters.

[18] To investigate the characteristics of this coupling during other solar activity levels, similar analysis was also carried out for the year 2012 (right panels). One can see a mixed situation in the data observed for this year wherein the periodicities that correspond to both solar and lower atmosphere are present in the upper atmosphere. The 5–6 day periodicity is present in all the atmospheric parameters including TEC; the 8–10 day period, which is dominant in the 10 hPa wind, is also present in other atmospheric parameters (though below the 90% FAL). Detailed analysis of solar

irradiance shows that there exist various short-term periodicities of 7, 9, 10, 15, 19, 21, 22, 23, 24, 25, and 26 days which may be due to the variation of the sunspot areas [see, e.g., *Willson*, 1982]. One can see here that in 2012, the Lomb-Scargle periodogram of the sunspot number also has significant power in the 8–9 and 12–13 day periodicities. Thus, the period of 13–15 days in the TEC and optical emissions could be an effect due to the solar forcings as well. Especially, in this period range, the periodicities seen in the upper atmosphere are also present in the data sets of the 10 hPa level zonal wind and the EEJ. This indicates possible influence from both solar forcing from above and lower atmospheric wave forcing from below on the upper atmosphere, and therefore, the relative effects cannot be obtained unambiguously as these two are convolved effects.

[19] Figure 5 shows that there are several wave periodicities that are common to both the lower atmospheric and upper atmospheric parameters. The Lomb-Scargle periodograms provide information on the presence of a particular frequency in a given data set, but not the time of occurrence of a particular frequency. To investigate whether the periodicities obtained in the different independent measurements are, if at all, simultaneous in their duration of occurrence, wavelet analysis is performed on all the individual data sets. Here for the estimation of the wavelet spectra, Morlet mother wavelet function is used [*Torrence and Compo*, 1998]. For optical data, the analysis is restricted to only that duration when almost continuous data are available (with at most two missing data points being interpolated). For 2011, DOY 7–46 and, for 2012, DOY 51–85 are used for the wavelet analysis. Figure 6 shows the wavelet spectra of all the data sets shown in Figure 5. Figures 6a–6g show the result of the wavelet analysis of SSN, TEC, OI 777.4 nm emission, OI 630.0 nm emission, OI 557.7 nm emission, EEJ, and 10 hPa zonal wind, respectively, for 2011. The right panels show the wavelet spectra of the corresponding parameters for 2012. The x axis shows the DOY and the y axis represents periods in days. Normalized power values are plotted in each panel and the scale is given on the right. It is striking to note that several periodicities, 5–6, 8–11, and quasi-16 days, are seen nearly simultaneously in almost all the atmospheric measurements in 2011 during DOY 20–45. The results arrived at from this analysis add credence to the suggestion that there seems to be a significant influence of lower atmospheric forcing on the upper atmospheric wave dynamics. As can be seen in Figures 5 and 6, the solar influence is significant only on the TEC variations in 2011.

[20] For 2012, the occurrence of 5 and 10 day periodicities in similar duration (DOY 50–85) in TEC, all the optical emissions, the EEJ strength, and the 10 hPa zonal wind shows the influence of the lower atmosphere-related processes in the upper atmospheric regions. The quasi-16 day period is present simultaneously in all the atmospheric parameters: 10 hPa zonal wind, EEJ strength, and TEC between DOY 5 and 30. SSN also has a significant period of 10–15 days in the same duration. This simultaneous presence of quasi-16 day periodicity in atmospheric and solar parameters implies a possible influence both from lower atmosphere and solar activity. It may be noticed that there is a broad similarity in the overall wavelet contours of EEJ, TEC, and SSN. Therefore, the broad picture that seems to emerge is that, the influences of both solar and lower atmospheric regions are seen to exist in the upper atmosphere in 2012, as opposed to 2011.

[21] There was a minor SSW event starting from DOY 32 in 2011 (shown by vertical dashed lines in Figure 6), when the temperature at 60°N latitude and at 10 hPa pressure level increased by more than 35°C within a week but the zonal wind did not reverse, indicating that the event was a minor one. It is important to note that several of the wave dynamical features (such as waves of 8–11 and quasi-16 days) occurred simultaneously even before the arrival of the minor SSW, which indicates that the vertical coupling of atmospheres in low solar activity exists, irrespective of the occurrence of the minor SSW event. Similar was the case for the minor SSW event starting from DOY 18 in 2012.

[22] The combined optical, radio, and magnetometer results presented here show that the vertical coupling of atmospheres is stronger during low solar activity epoch (2011) when the average SSN was 35. In 2012, when the average SSN during our observation was 52, the effects of both the PW-associated activity and the solar activity are seen in the upper atmosphere. *Pallamraju et al*. [2010] presented optical dayglow data from 2001 (average SSN was 123) and showed that almost all of its variations were of solar origin and none from the lower (MLT) region dynamics as manifested in the EEJ. The upper atmospheric behavior has conventionally been considered to be varying solely under the influence of solar activity and to a much smaller degree on the lower atmospheric forcings. Our results reveal a broader picture wherein there seems to be an interplay between the influences of lower atmospheric processes and solar activity on the upper atmosphere. From the present results, it is proposed that lower atmospheric behavior influences the upper atmosphere at least until the SSN value of 35; there exists a transition from the influences of lower atmospheric origin to a mixed behavior between average SSNs of 35 and 52 and from the mixed effect to that of purely of solar origin between SSN values of 52 and 123. Further studies are required to ascertain these boundaries more quantitatively in terms of the number of sunspots.

[23] It is known that the PWs modulate the GWs and tides, which thereby affect the upper atmosphere. Both neutral and plasma components are affected due to such secondary effects of planetary waves especially in the equatorial region. From modeling studies, *Liu et al*. [2010] have shown that the GWs are more favorable to propagate to altitudes up to 150 km during low solar activity period. Using numerical simulations, *Wan et al*. [2012] have shown that the neutral coupling of the atmosphere via nonmigrating diurnal eastward wave number 3 tidal influence decreases with increasing solar activity, while the electrodynamical coupling remains unchanged. Those results suggest that during higher solar activity, the influence of PW to the upper atmosphere would be minimum, which is similar to the result reported in this study. Further, our detailed investigations using measurements of multiple data sets not only provide empirical evidence to the conjectures and modeling studies reported earlier but also characterize the strength of the vertical coupling of atmospheres from lower to higher altitudes—which is much stronger in the low solar activity epoch than in the high solar activity period.

[24] Further, there are reports on the influence of the lower atmospheric forcing (via PWs) on the upper atmospheric

dynamics even in the high solar activity epochs (wherein the SSN varied between 60 and 110) [e.g., *Liu and Roble*, 2005; *Liu et al*., 2010; *Pedatella and Forbes*, 2010]. On closer scrutiny, we found that even though the solar activity was high, the lower atmospheric forcings on the upper atmosphere occurred mainly during SSW events only, as most likely the warming events provided additional sources of energy. Based on our present results and simulation studies of *Wan et al*. [2012], it can be seen that the temperature gradients in the MLT height region play an important role in the lower atmospheric wave propagation to the upper atmosphere. In summary, our study indicates that the atmospheric conditions are favorable for waves to propagate vertically in the low solar activity epoch. If there are SSW events during such period, it would enhance the strength of the propagation of waves enabling a stronger vertical coupling of atmospheres. During high solar activity epochs, the upper atmospheric dynamics are predominantly controlled by those of solar flux variability and not of those due to the PW-type effects from the lower altitudes. However, SSW events during high solar activity period can enable vertical couplings from below.

4. Summary and Conclusions

[25] Systematic and continuous ground-based dayglow emission intensities over a large FOV for around 2.5 years have been obtained from a low-latitude station, Hyderabad, India. Data during January–March of 2011 and 2012 are investigated to study the relative importance of the influences of the lower atmospheric forcing versus that of solar on the upper atmospheric wave dynamics. In addition to the neutral dynamical parameters such as the zonal wind at 10 hPa and dayglow, the EEJ strength and the GPS-TEC data are used to study the electrodynamic behavior of the upper atmosphere. Data observed from multiple instruments showed that the PW-type oscillations of periods 5–6, 8–11, quasi-16, and 25 days influence the upper atmosphere not only through the electrodynamic coupling but also through the neutral atmospheric coupling, as all the neutral and plasma parameters bear the signatures of these oscillations. The relative importance of the forcing from below and from above due to direct solar forcing is found to be varying with the strength of solar activity. Lower atmospheric influences on the upper atmosphere are found to be stronger during the low solar activity period of 2011 compared to the moderate solar activity period of 2012. Dayglow data of the high solar activity period (2001) showed a clear correlation in the behavior of the upper atmosphere with that of the direct solar forcing but weaker to no influence from lower atmospheric wave activity on the upper atmospheric neutral behavior. Based on the influence/presence of PWs on the atmospheric parameters and on the level of solar activity for the three different activity phases, it is proposed that (i) the effect on upper atmospheric dynamics due to the lower atmosphere exists at least until the average SSN is 35, (ii) there is a transition from the lower atmospheric forcing to mixed behavior between average SSNs of 35 and 52, and (iii) there is a transition from mixed effects to those purely of solar origin between SSN values of 52 and 123. Further, epochs of SSW activity may enhance the coupling from below even when the solar activity is high.

[26] **Acknowledgments.** The authors acknowledge the assistance of Srikanth and Hema at JNTU, Hyderabad, in arranging the logistics and maintaining the Aeronomy laboratory. We would like to place on record our gratitude to the late R. Raghavarao for initiating the PRL-JNTUH collaborative work. Thanks are due to the Director of PRL and Vice-Chancellor of JNTUH for fostering this collaboration. Discussions with R. Sekar and R. Sridharan were very helpful. The sunspot number data are obtained from NASA-OMNIWeb. The RINEX format GPS observational and navigational data are obtained from the International GNSS Service (IGS) network. The work at the University of Massachusetts Lowell was supported by Office of Naval Research grant N00014-13-1-0266 and NSF CEDAR grant AGS-1315354. This work is supported by the Department of Space, Government of India.

[27] Robert Lysak thanks Hisao Takahashi and Helen Parish for their assistance in evaluating this paper.

References

Abdu, M., T. Ramkumar, I. Batista, C. Brum, H. Takahashi, B. Reinisch, and J. Sobral (2006), Planetary wave signatures in the equatorial atmosphere-ionosphere system, and mesosphere-*E*- and *F*-region coupling, *J. Atmos. Sol.-Terr. Phys.*, *68*(3-5), 509–522, doi:10.1016/j.jastp.2005.03.019.

Barth, C. A., and A. F. Hildebrandt (1961), The 5577 Å airglow emission mechanism, *J. Geophys. Res.*, *66*(3), 985–986, doi:10.1029/JZ066i003p00985.

Chau, J., L. Goncharenko, B. Fejer, and H.-L. Liu (2012), Equatorial and low latitude ionospheric effects during sudden stratospheric warming events, *Space Sci. Rev.*, *168*, 385–417, doi:10.1007/s11214-011-9797-5.

Delbouille, L., L. Neven, and G. Roland (1973), *Photometric Atlas of the Solar Spectrum From Lambda 3000 to Lambda 10000: 2994-6455*, vol. 1, Inst. d'Astrophysique de L'Univ, Cointe-Ougreé, Belgium.

Dow, J., R. Neilan, and C. Rizos (2009), The International GNSS Service in a changing landscape of global navigation satellite systems, *J. Geod.*, *83*, 191–198, doi:10.1007/s00190-008-0300-3.

Fejer, B. (2011), Low latitude ionospheric electrodynamics, *Space Sci. Rev.*, *158*, 145–166, doi:10.1007/s11214-010-9690-7.

Forbes, J. (1982), Atmospheric tides: 1. Model description and results for the solar diurnal component, *J. Geophys. Res.*, *87*(A7), 5222–5240.

Forbes, J., M. Hagan, S. Miyahara, F. Vial, A. Manson, C. Meek, and Y. Portnyagin (1995), Quasi 16-day oscillation in the mesosphere and lower thermosphere, *J. Geophys. Res.*, *100*(D5), 9149–9163.

Fritts, D. C., and M. J. Alexander (2003), Gravity wave dynamics and effects in the middle atmosphere, *Rev. Geophys.*, *41*(1), 1003, doi:10.1029/2001RG000106.

Goncharenko, L. P., J. L. Chau, H.-L. Liu, and A. J. Coster (2010), Unexpected connections between the stratosphere and ionosphere, *Geophys. Res. Lett.*, *37*, L10101, doi:10.1029/2010GL043125.

Goncharenko, L. P., V. W. Hsu, C. G. M. Brum, S.-R. Zhang, and J. T. Fentzke (2013), Wave signatures in the mid-latitude ionosphere during a sudden stratospheric warming of January 2010, *J. Geophys. Res. Space Physics*, *118*, 472–487, doi:10.1029/2012JA018251.

Grainger, J., and J. Ring (1962), Anomalous Fraunhofer line profiles, *Nature*, *193*, 762, doi:10.1038/193762a0.

Guharay, A., and R. Sekar (2012), Signature of latitudinal coupling during a major sudden stratospheric warming in the tropics, *J. Atmos. Sol.-Terr. Phys.*, *75*, 122–126.

Gurubaran, S., S. Sridharan, T. Ramkumar, and R. Rajaram (2001), The mesospheric quasi-2-day wave over Tirunelveli (8.7°N), *J. Atmos. Sol.-Terr. Phys.*, *63*(10), 975–985, doi:10.1016/S1364-6826(01)00016-5.

Harris, R., and R. Mach (2007), The GPSTk: An open source GPS toolkit, *GPS Solut.*, *11*, 145–150, doi:10.1007/s10291-006-0043-7.

Hines, C. O. (1960), Internal atmospheric gravity waves at ionospheric heights, *Can. J. Phys.*, *38*, 1441.

Hocke, K., and K. Schlegel (1996), A review of atmospheric gravity waves and travelling ionospheric disturbances: 1982–1995, *Ann. Geophys.*, *14*, 917–940, doi:10.1007/s00585-996-0917-6.

Horne, J. H., and S. L. Baliunas (1986), A prescription for period analysis of unevenly sampled time series, *Astrophys. J.*, *302*, 757–763, doi:10.1086/164037.

Immel, T. J., E. Sagawa, S. L. England, S. B. Henderson, M. E. Hagan, S. B. Mende, H. U. Frey, C.M. Swenson, and L. J. Paxton (2006), Control of equatorial ionospheric morphology by atmospheric tides, *Geophys. Res. Lett.*, *33*, L15108, doi:10.1029/2006GL026161.

Kalnay, E., et al. (1996), The NCEP/NCAR 40-year reanalysis project, *Bull. Am. Meteorol. Soc.*, *77*(3), 437–471, doi:10.1175/1520-0477(1996)077<0437:TNYRP>2.0.CO;2.

Kulkarni, P. V. (1976), Rocket study of 5577 Å OI emission at night over the magnetic equator, *J. Geophys. Res.*, *81*(22), 3740–3744, doi:10.1029/JA081i022p03740.

Liu, H. L., and R. G. Roble (2005), Dynamical coupling of the stratosphere and mesosphere in the 2002 Southern Hemisphere major stratospheric

sudden warming, *Geophys. Res. Lett.*, *32*, L13804, doi:10.1029/2005GL022939.

Liu, H.-L., W. Wang, A. D. Richmond, and R. G. Roble (2010), Ionospheric variability due to planetary waves and tides for solar minimum conditions, *J. Geophys. Res.*, *115*, A00G01, doi:10.1029/2009JA015188.

Lomb, N. R. (1976), Least-squares frequency analysis of unequally spaced data, *Astrophys. Space Sci.*, *39*, 447–462, doi:10.1007/BF00648343.

Matsuno, T. (1971), A dynamical model of the stratospheric sudden warming, *J. Atmos. Sci.*, *28*(8), 1479–1494, doi:10.1175/1520-0469(1971)028<1479:ADMOTS>2.0.CO;2.

Meyer, C. K., and J. M. Forbes (1997), A 6.5 day westward propagating planetary wave: Origin and characteristics, *J. Geophys. Res.*, *102*(D22), 26,173–26,178.

Nanan, B., C. Chen, P. Rajesh, J. Liu, and G. Bailey (2012), Modeling and observations of the low latitude ionosphere-plasmasphere system at long deep solar minimum, *J. Geophys. Res.*, *117*, A08316, doi:10.1029/2012JA017846.

Niranjan Kumar, K., A. Taori, S. Sathishkumar, V. Kamalakar, R. Ghodpage, S. Gurubaran, P. T. Patil, S. V. B. Rao, and A. K. Patra (2012), On the linkage of mesospheric planetary waves with those of the lower atmosphere and ionosphere: A case study from Indian low latitudes, *J. Geophys. Res.*, *117*, A11303, doi:10.1029/2012JA018139.

Pallam Raju, D., R. Sridharan, S. Gurubaran, and R. Raghavarao (1996), First results from ground-based daytime optical investigation of the development of the equatorial ionization anomaly, *Ann. Geophys.*, *14*(2), 238–245, doi:10.1007/s00585-996-0238-9.

Pallamraju, D., and S. Chakrabarti (2005), First ground-based measurements of OI 6300 Å daytime aurora over Boston in response to the 30 October 2003 geomagnetic storm, *Geophys. Res. Lett.*, *32*, L03S10, doi:10.1029/2004GL021417.

Pallamraju, D., J. Baumgardner, and S. Chakrabarti (2000), A multiwavelength investigation of the ring effect in the day sky spectrum, *Geophys. Res. Lett.*, *27*(13), 1875–1878.

Pallamraju, D., J. Baumgardner, and S. Chakrabarti (2002), HIRISE: A ground-based high-resolution imaging spectrograph using echelle grating for measuring daytime airglow/auroral emissions, *J. Atmos. Sol.-Terr. Phys.*, *64*, 1581–1587, doi:10.1016/S1364-6826(02)00095-0.

Pallamraju, D., S. Chakrabarti, and C. E. Valladares (2004), Magnetic storm-induced enhancement in neutral composition at low latitudes as inferred by O(^{1}D) dayglow measurements from Chile, *Ann. Geophys.*, *22*(9), 3241–3250, doi:10.5194/angeo-22-3241-2004.

Pallamraju, D., U. Das, and S. Chakrabarti (2010), Short- and long-timescale thermospheric variability as observed from OI 630.0 nm dayglow emissions from low latitudes, *J. Geophys. Res.*, *115*, A06312, doi:10.1029/2009JA015042.

Pallamraju, D., G. Lu, and C. Lin (2012), Overview of the special issue on the atmospheric coupling processes in the Sun-Earth system, *J. Atmos. Sol-Terr. Phys.*, *75–76*, 1–4.

Pallamraju, D., F. I. Laskar, R. P. Singh, J. Baumgardner, and S. Chakrabarti (2013), MISE: A multiwavelength imaging spectrograph using echelle grating for daytime optical aeronomy investigations, *J. Atmos. Sol.-Terr. Phys.*, doi:10.1016/j.jastp.2012.12.003, in press.

Pancheva, D., et al. (2008), Planetary waves in coupling the stratosphere and mesosphere during the major stratospheric warming in 2003/2004, *J. Geophys. Res.*, *113*, D12105, doi:10.1029/2007JD009011.

Parish, H. F., J. M. Forbes, and F. Kamalabadi (1994), Planetary wave and solar emission signatures in the equatorial electrojet, *J. Geophys. Res.*, *99*(A1), 355–368, doi:10.1029/93JA02096.

Pedatella, N. M., and J. M. Forbes (2010), Evidence for stratosphere sudden warming ionosphere coupling due to vertically propagating tides, *Geophys. Res. Lett.*, *37*, L11104, doi:10.1029/2010GL043560.

Pogoreltsev, A., A. Vlasov, K. Frohlich, and C. Jacobi (2007), Planetary waves in coupling the lower and upper atmosphere, *J. Atmos. Sol.-Terr. Phys.*, *69*(17), 2083–2101.

Prakash, S., D. Pallamraju, and H. S. S. Sinha (2009), Role of the equatorial ionization anomaly in the development of the evening prereversal enhancement of the equatorial zonal electric field, *J. Geophys. Res.*, *114*, A02301, doi:10.1029/2007JA012808.

Raghavarao, R., M. Nageswararao, J. H. Sastri, G. D. Vyas, and M. Sriramarao (1988), Role of equatorial ionization anomaly in the initiation of equatorial spread *F*, *J. Geophys. Res.*, *93*(A6), 5959–5964, doi:10.1029/JA093iA06p05959.

Rama Rao, P. V. S., K. Niranjan, D. S. V. V. D. Prasad, S. Gopi Krishna, and G. Uma (2006), On the validity of the ionospheric pierce point (IPP) altitude of 350 km in the Indian equatorial and low-latitude sector, *Ann. Geophys.*, *24*(8), 2159–2168, doi:10.5194/angeo-24-2159-2006.

Salby, M. L. (1984), Survey of planetary-scale travelling waves: The state of theory and observations, *Rev. Geophys.*, *22*(2), 209–236, doi:10.1029/RG022i002p00209.

Sassi, F., R. Garcia, and K. Hoppel (2012), Large-scale Rossby normal modes during some recent Northern Hemisphere winters, *J. Atmos. Sci.*, *69*(3), 820–839.

Solomon, S. C., and V. J. Abreu (1989), The 630 nm dayglow, *J. Geophys. Res.*, *94*(A6), 6817–6824, doi:10.1029/JA094iA06p06817.

Sridharan, R., D. P. Raju, R. Raghavarao, and P. V. S. Ramarao (1994), Precursor to equatorial spread-F in OI 630.0 nm dayglow, *Geophys. Res. Lett.*, *21*(25), 2797–2800, doi:10.1029/94GL02732.

Sripathi, S., and A. Bhattacharyya (2012), Quiet time variability of the GPS TEC and EEJ strength over Indian region associated with major sudden stratospheric warming events during 2005/2006, *J. Geophys. Res.*, *117*, A05305, doi:10.1029/2011JA017103.

Takahashi, H., R. Buriti, D. Gobbi, and P. Batista (2002), Equatorial planetary wave signatures observed in mesospheric airglow emissions, *J. Atmos. Sol.-Terr. Phys.*, *64*(811), 1263–1272, doi:10.1016/S1364-6826(02)00040-8.

Torrence, C., and G. P. Compo (1998), A practical guide to wavelet analysis, *Bull. Amer. Meteorol. Soc.*, *79*(1), 61–78, doi:10.1175/1520-0477(1998)079<0061:APGTWA>2.0.CO;2.

Valladares, C. E., S. Basu, K. Groves, M. P. Hagan, D. Hysell, A. J. Mazzella, and R. E. Sheehan (2001), Measurement of the latitudinal distributions of total electron content during equatorial spread F events, *J. Geophys. Res.*, *106*(A12), 29,133–29,152, doi:10.1029/2000JA000426.

Vineeth, C., T. K. Pant, C. V. Devasia, and R. Sridharan (2007), Atmosphere-ionosphere coupling observed over the dip equatorial MLTI region through the quasi 16 day wave, *Geophys. Res. Lett.*, *34*, L12102, doi:10.1029/2007GL030010.

Wan, W., Z. Ren, F. Ding, J. Xiong, L. Liu, B. Ning, B. Zhao, G. Li, and M.-L. Zhang (2012), A simulation study for the couplings between DE3 tide and longitudinal WN4 structure in the thermosphere and ionosphere, *J. Atmos. Sol.-Terr. Phys.*, *90-91*, 52–60, doi:10.1016/j.jastp.2012.04.011.

Willson, R. C. (1982), Solar irradiance variations and solar activity, *J. Geophys. Res.*, *87*(A6), 4319–4326, doi:10.1029/JA087iA06p04319.

Zhang, S. P., and G. G. Shepherd (2004), Solar influence on the O(^{1}D) dayglow emission rate: Global-scale measurements by WINDII on UARS, *Geophys. Res. Lett.*, *31*, L07804, doi:10.1029/2004GL019447.

Zhang, S. P., and G. G. Shepherd (2005), On the response of the O(^{1}S) dayglow emission rate to the Sun's energy input: An empirical model deduced from WINDII/UARS global measurements, *J. Geophys. Res.*, *110*, A03304, doi:10.1029/2004JA010887.